Available online at www.sciencedirect.com
ScienceDirect
Nuclear Instruments and Methods in Physics Research A 576 (2007) 422–429
NUCLEAR INSTRUMENTS & METHODS IN PHYSICS RESEARCH Section A
www.elsevier.com/locate/nima

In situ visualization of thermal distortions of synchrotron radiation optics

P. Revesz*, A. Kazimirov, I. Bazarov

Cornell High Energy Synchrotron Source (CHESS), 200L Wilson Laboratory, Cornell University, Ithaca, NY 14850, USA

Received 12 February 2007; received in revised form 13 February 2007; accepted 24 February 2007
Available online 12 March 2007

Abstract

We have developed a new in situ method to measure heating-induced distortions of the surface of the first monochromator crystal exposed to high-power white synchrotron radiation beam. The method is based on recording the image of a stationary grid of dots captured by a CCD camera as reflected from the surface of a crystal with and without a heat load. The three-dimensional surface profile (heat bump) is then reconstructed from the distortions of the original pattern. In experiments performed at the CHESS A2 wiggler beam line we measured the heat bumps with the heights of up to 600 nm produced by a wiggler beam with total power in the range of 15–60 W incident on the (1 1 1) Si crystal at various angles between 3° and 15°.

PACS: 07.85.Qe; 65.40.De; 42.87.−d

Keywords: Synchrotron radiation; High heat-load optics; Heat bump; Surface profile measurement; Optical metrology

1. Introduction

High heat load of the optical elements of modern synchrotron radiation (SR) beam lines under powerful undulator or wiggler beams is one of the main factors limiting available photon flux for experiment. Thermal distortions of the lattice of the first crystal, typically Si, due to the inhomogeneous absorption of the incident white or pink beam in the bulk of the crystal lead to a broadening of the rocking curve and reduction in peak intensity. Sophisticated cooling techniques such as liquid N_2 cooling [1] have been developed at the 3rd generation SR sources to minimize this effect. The heat load problem is expected to be more severe at the next generation sources.

Almost all studies of crystals under high heat load so far were performed by measuring an X-ray response, i.e. a double crystal rocking curve, which is a convolution of the first, distorted, crystal with the second perfect crystal. That produces an integral over the footprint of the beam characteristic with all the details of the complex thermal distortion distribution lost. Our understanding of the heat problem would benefit significantly if we could be able to measure the shape of the surface of the first crystal or multilayer, i.e. the so called heat bump, in situ under the high heat load.

There are several approaches to visualizing distorted surfaces. Flatness of a reflecting surface can be evaluated with micro-radian accuracy over a large area using optical methods such as the long trace profiler (LTP), as Takacs et al. demonstrated [2–3]. It measures the surface slope along a line of a mirror. The method uses a laser beam reflected from the test surface and the reference mirror. Part of the optical system is mounted on a precision translation stage to scan along the mirror surface. Takacs's method showed excellent accuracy of slope error (deviation from the ideal flat) measurement and it was used also to measure a heat-bump profile on a beam line mirror surface as a result of a ~100 W X-ray radiation. To recover the shape of a weld-pool in three dimensions, Saeed et al. [4] used a laser beam reflected from the surface. In his measurement, the reflected beam was captured with a CCD camera and the positions of the laser spots were analyzed to reconstruct the weld-pool surface. In Saeed's experiment, the typical weld-pool

*Corresponding author. Fax: +1 607 255 9001.
E-mail address: pr20@cornell.edu (P. Revesz).

0168-9002/$ - see front matter © 2007 Elsevier B.V. All rights reserved.
doi:10.1016/j.nima.2007.02.110

depth was in the tens of microns range and probed surface area was $3.5 \times 1.5\,mm^2$.

The LTP method provides excellent accuracy in determining surface shapes, however, it only provides information along a line. In the case of SR optics under the white beam the typical heat-bump results in a slope error in the range of a few tens of micro-radians and the affected area is a few square centimeters. In this work, a new optical technique based on analyzing an optical image of a periodic rectangular array reflected by a mirror surface of the distorted crystal is presented and first experimental results of a direct measurement of three-dimensional (3-D) heat-bump surface profiles under a wiggler beam are discussed.

2. Technique description

The principle diagram of our setup is shown in Fig. 1. A flat panel light source covered by a thin metal shield with an array of small holes served as an object to be imaged. The video camera captures the image of the light-dot array reflected from the optically polished first crystal of the monochromator. The spacing between the holes was 1.5 mm and hole diameter was 0.3 mm. A total of 4×4 in. area was covered by the array of holes. This dot array light source was placed inside the monochromator box replacing the second crystal. To capture the image of the dot array light source we have used a high-sensitivity Astrovid CCD camera with a 55 mm telecentric lens.

The heat-bump measurement was done at the CHESS A2 beam line fed by a 49-pole wiggler. We used a 10 mm thick, 2×4 in. Si$\langle 1\,1\,1 \rangle$ crystal. The crystal was attached to a water-cooled copper substrate covered by liquid Indium for better thermal contact. During the experiment the crystal angle varied between 4° and 15° thereby varying the beam footprint and X-ray power density hitting the crystal. In addition, the beam defining slit sizes were varied from 0.3×3 mm to 0.6×6 mm (the dimensions are vertical-by-horizontal). The total white beam power impinging the crystal surface varies between 15 and 60 W, depending on the entrance slit size of the monochromator. The Astrovid CCD camera was mounted on top of the monochromator box and the images were captured through a high-vacuum view-port. In our experimental setup the camera views only a portion of the dot array (on average 20×30 dots) and only a portion of the total surface of the Si crystal (on average a $20 \times 30\,mm^2$ area). This coverage is mainly determined by the camera-crystal and crystal-light source distances as well as the optics used.

To measure the change in position of each dot of the array we have used a modified version of the program *Centroid* described earlier [5]. This program analyzes each captured frame and calculates the (x, y) position coordinates based upon center-of-gravity (COG) calculations for the pixel intensities within a region of interest. The accuracy of the position determination has been shown to be better than a micron. In the case of the dot array light source used for heat-bump measurement the COG of each light dot is calculated. As part of the surface distorts, as a result of the beam heating, it acts as a distorted mirror, the dots will move away from their original position depending on the amount of distortion. As long as the distance between the optical elements is constant, the change in dot positions Δx, Δy is proportional to the change in the slope angle of the surface $\Delta\theta_x$, $\Delta\theta_y$. The fact that the crystal is mounted on a precise goniometer offers an easy and accurate way to calibrate the measuring system by introducing a small calibrating tilt motion of the crystal and recording the observed change in the position of the dots. The *Centroid* program will generate an array containing $\Delta\theta_x$, $\Delta\theta_y$ for each light dot point—the slope error vector map. Calculation of the slope vector map is done using a fixed rectangular grid array encompassing each dot. (Unlike [4], where the laser dots were followed with a sophisticated tracking algorithm.) Thus, the COG calculation was carried out for each grid cell resulting in

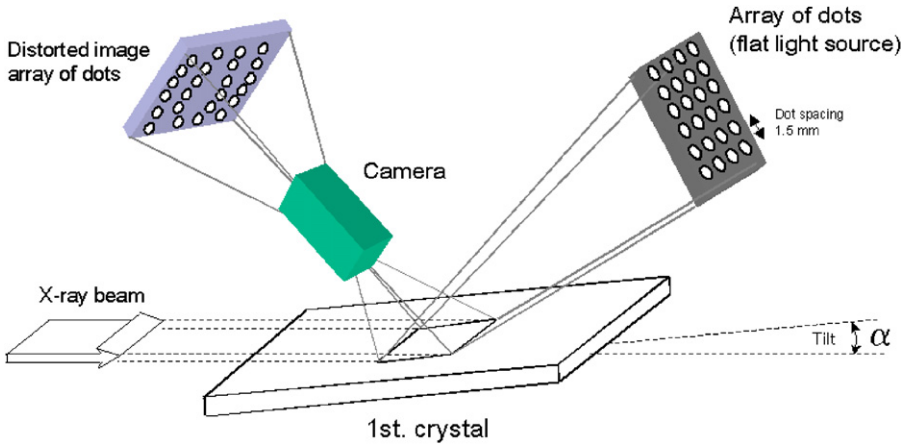

Fig. 1. Principal scheme of heat-bump measurement. The image of an array of light-dots is captured with a CCD camera as reflected from the crystal. The position of the dots in the image shifts as the crystal becomes deformed as a result of beam heating.

the slope vector map. The slope vector map is displayed on-the-fly by *Centroid* as a vector map as well as being saved for further data analysis. In order to improve the signal-to-noise ratio of the video data collection, for each slope error vector map 10 captured frames were averaged, and for each frame median filtering was applied to minimize the effects of "zingers" (attributed to random extreme pixel values due to scattered X-rays.) The advantage of using median filtering of the image (in our case a 3×3 median matrix was used) is that it alters single pixels that stand out from their surrounding. We apply the median filter for each captured frame thus avoiding the possibility of joining "zingers" to extend over multiple pixels. On the other hand, the effect of a local hotspot on the surface will extend laterally to a distance of $\sim(D\tau)^{1/2}$ where D is the thermal diffusivity of silicon ($\sim 0.5\,\mathrm{cm^2\,s^{-1}}$) and τ is a characteristic measurement time. Even in the best case, when the heat bump is measured for each captured frame (1/30 s) the thermal diffusivity of Si will "smear" a hotspot over thousands of microns corresponding many pixels in the image thus unaltered by the median filtering.

It has been shown in Ref. [5] that the measurement of a centroid position of a light spot using an 8-bit CCD cameras can be done with sub-micron accuracy. There is a simple, linear relation between the apparent change of the position Δ of the light dots and the change in the angle α of the reflecting surface: $\alpha = \Delta/L$, where L is the total path length between the light dots and the camera. Therefore, the x and y components of changes in the slope vector of the reflecting surface are directly proportional to the observed changes of the light dots in the x and y directions. Because the crystal is mounted on a goniometer the calibration of the optical elements for the slope vector measurement can be done conveniently by producing a known increment of crystal tilt (we used 50 μrad) of the reflecting crystal and measuring the shift of the light dots.

The minimum detectable change in the slope of the reflecting surface is directly related to the minimum detectible change in centroid position of the light dots. This in one hand is determined by quality and signal-to-noise ratio of the image captured, on the other hand, by the amount of demagnification of the optical system. In our present configuration, the position measurement of the light dots was determined with an accuracy of $\sigma \sim 0.8\,\mu\mathrm{m}$. This translates to an accuracy of $\sigma' < 2\,\mu\mathrm{rad}$ for the measurement of slope error vector. The 2 μrad slope error translates to 20 nm variations in height when measured with a $1 \times 1\,\mathrm{mm}^2$ grid spacing.

Increasing the area to be surveyed requires optics with wider angle of view (thus greater demagnification of the image) resulting in worsening the detection limits.

The amount of the largest distortion of the reflecting surface that can be measured is determined by the maximum centroid movement of a light dot without leaving its sub-cell. In out experimental conditions, this amounts to a maximum slope error of ~1000 μrad.

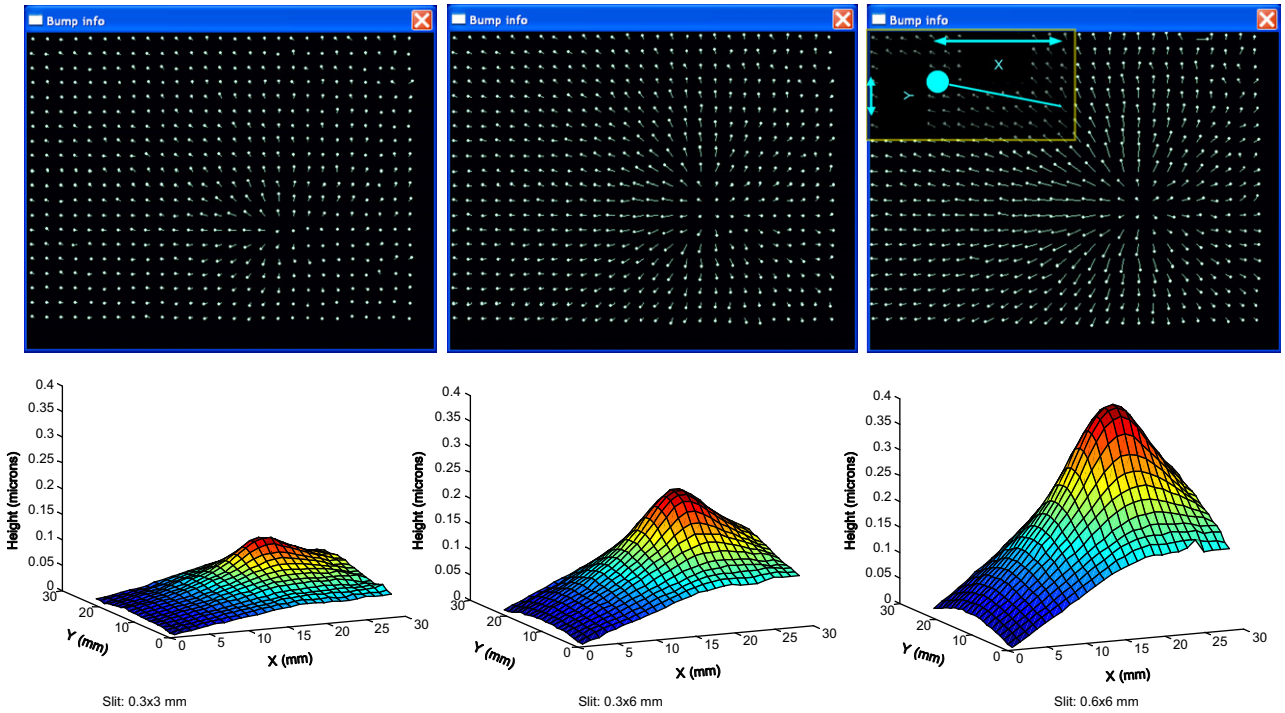

Fig. 2. Crystal tilted 5°, shown for three sizes of slit openings, as indicated. The X-ray direction is from the left. On the top, the dot arrays represent the position of each light dot. The relative (to no heat load position) shift of each dot is shown with a line. ΔX and ΔY are the X and Y components of the position shift, proportional to the slope error at a particular position on the crystal. On the bottom, the calculated heat-bump surfaces are shown. The vertical scales of the heat-bump height shown in microns. Note that the scale is exaggerated in the vertical direction.

3. Experimental results

In Fig. 2, on the top panel, the slope error vector map is shown (actual screen dumps from *Centroid*) and below is the reconstructed 3-D surface of the crystal showing the heat bump for three beam defining slit sizes at 5° tilt angle. The inset in the slope error vector map explains the meaning of the individual slope vectors. The nominal power impinging the Si crystal at slit sizes (vertical × horizontal) of 0.3×3, 0.3×0.6 and $0.6 \times 6\,mm^2$ was 15.2, 30.3 and 60.3 W, respectively, as calculated using XOP taking into account the wiggler parameters, X-ray absorption carbon filters, Beryllium windows and experimental geometry. The vertical scales for the 3-D plots are the same for all slit sizes so it is easier to see the changes in the bump surface. The height of the bump, as expected, increases with the deposited total power. The heat-bump surface looks quite dramatic, especially with the slits fully open. Note however, displacement is a few hundred nanometers over a distance of tens of millimeters.

Another feature of the plots is that the heat-bump profile seems to be tilted (asymmetrical) as the deposited beam power increases. This behavior is related to the following: (1) the irradiated area of the crystal is off-center of the crystal making the deposited power distribution asymmetrical. (2) We obtain slope error vector maps from the shift of the position of the dots assuming the conversion factor to be constant (an average) for each light dot. This is not quite correct: light paths for the dots at the left-most versus the right-most light dots are slightly different. Assuming the conversion to be constant introduces a systematic error in the slope error vector maps, thus introducing some distortion of the heat-bump profile. Our measurements show that the maximum variation of the calibration factor is ~4%.

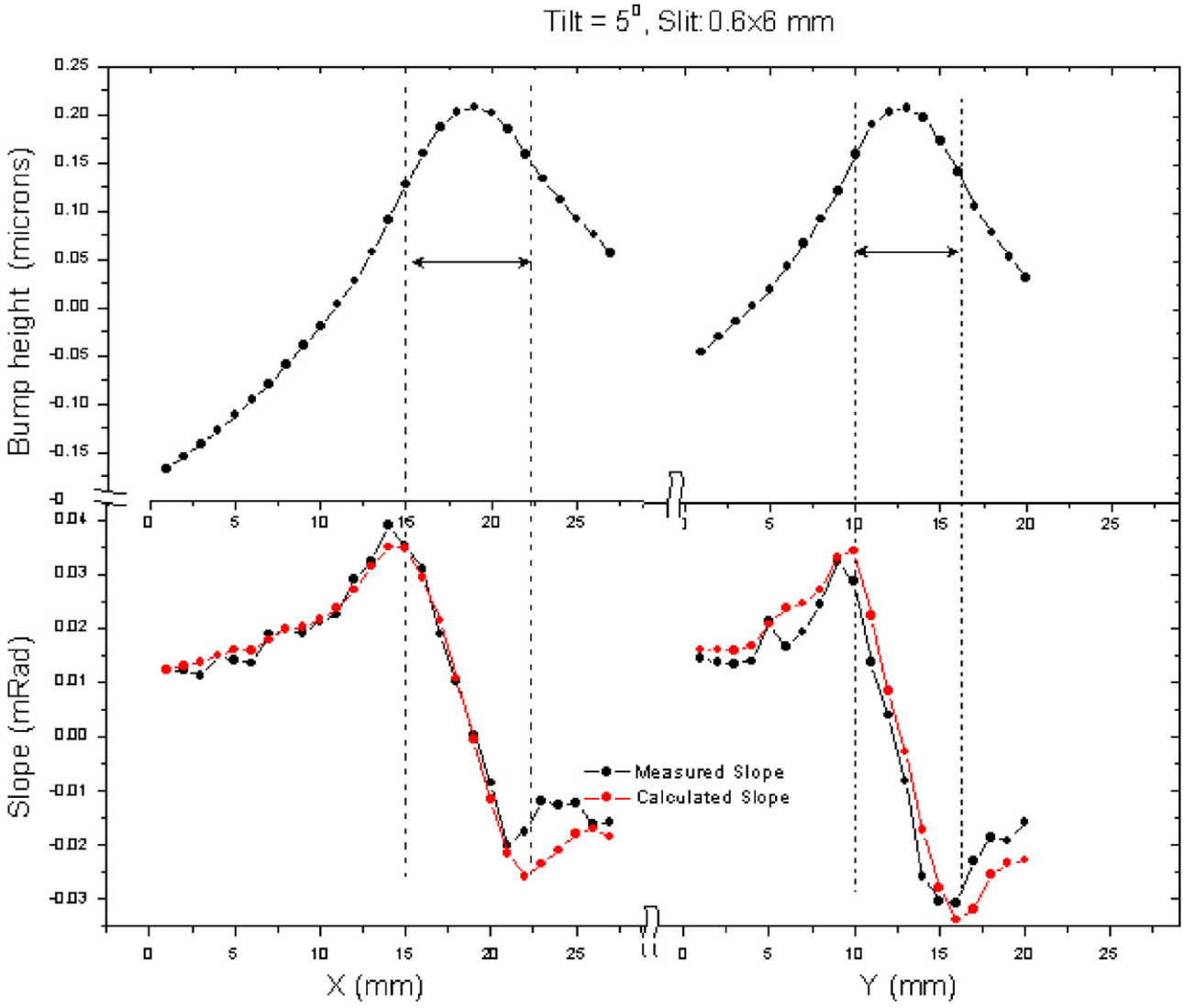

Fig. 3. Heat-bump height and slope errors are shown along the "crest" of the heat bump in X and Y directions for beam incidence at 5°. For the slope errors curves, the measured data (black) is compared with the slope errors re-calculated from the reconstructed heat-bump surfaces using the Poisson method (red).

In Figs. 3 and 4, the heat-bump height and slope error along the "crest" of the heat bump (in the direction and perpendicular to the beam) are shown for 5° and 14° incident angles, respectively. The dotted vertical lines represent the edges of the footprint of the X-ray beam (the X-ray beam hits the crystal only in the area between these lines). The locations of extreme values for the slope error are quite close to the edges of the radiated area. This is what one would expect: those are the locations where the heat gradient should be the greatest.

In Fig. 5, the effect of crystal tilt at fixed slit size on the heat-bumps formation is shown. The slit size is $0.6 \times 6\,\mathrm{mm}^2$ (vertical by horizontal) and the tilts are 5° and 14°. On the top the screen dump of the slope error vector map, on the bottom slope the reconstructed 3-D surface and contour plots are shown. The small rectangles on the contour plots show the footprint of the beam. The surface plots are shifted vertically for the better view of the contour plots. It is obvious from this figure that the heat-bump effect is especially severe at large tilts corresponding to low energy settings of the monochromator.

There are two slope error curves shown in Figs. 3 and 4: in black the slope error values as measured and in red as re-calculated from the reconstructed surface. In an ideal world, these two slope error curves would be identical. The basic difference between the measured (black) and the re-calculated slope errors is that the measured slope error curves looks noisier that the calculated ones. We have not used any smoothing procedures at the heat-bump surface calculations. The experimental procedure (as any experimental procedure would) introduces some error or noise in the slope error vector map data. The errors or noise in slope vector map data will result in a non-zero curl(**s**) distorting the integral, thus the reconstructed surface. As shown in the next section, the mathematical procedure used to calculate the surface minimizes certain experimental errors.

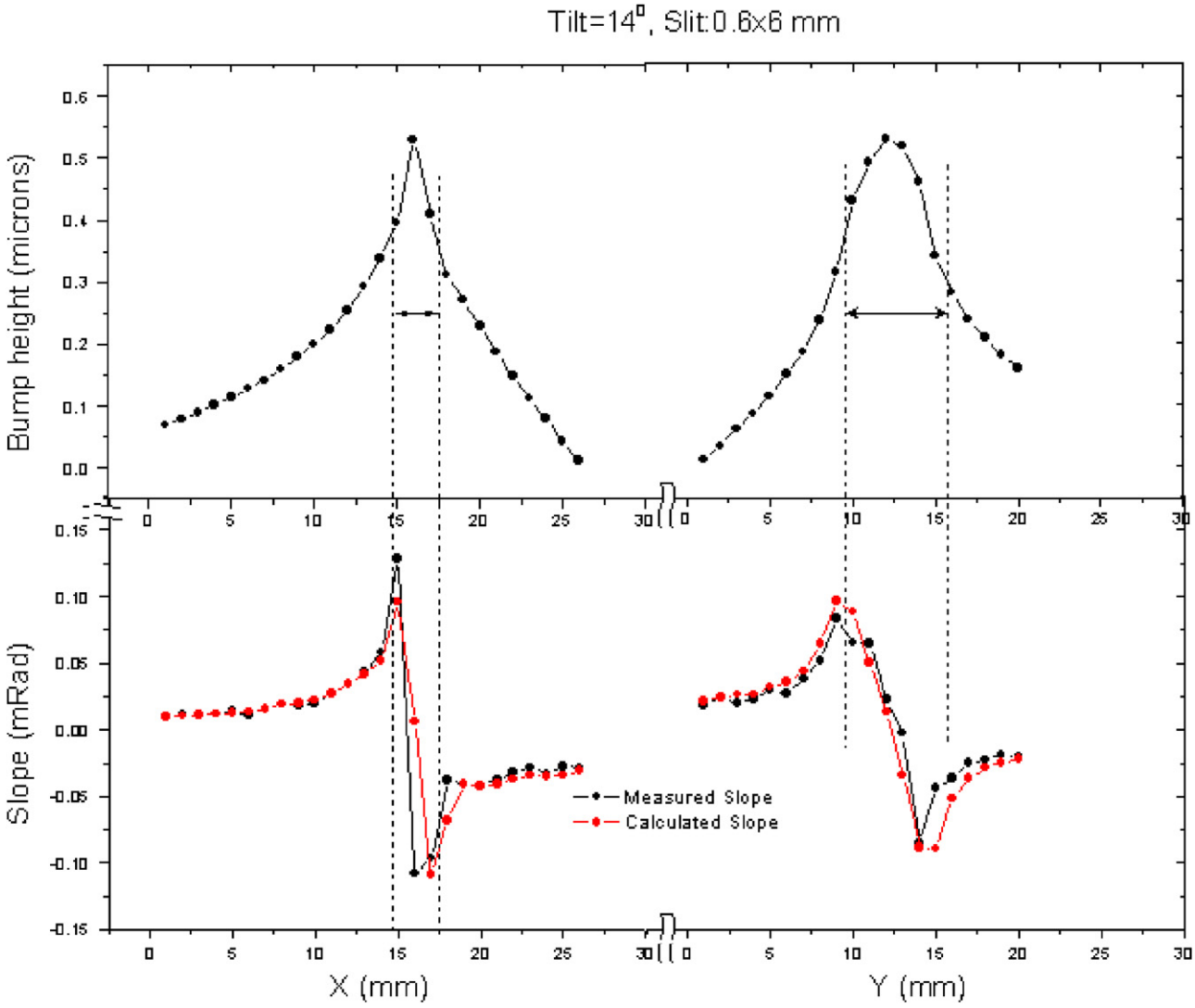

Fig. 4. Heat-bump height and slope errors are shown along the "crest" of the heat bump in X and Y directions for beam incidence at 14°. For the slope errors curves, the measured data (black) is compared with the slope errors re-calculated from the reconstructed heat-bump surfaces using the Poisson method (red).

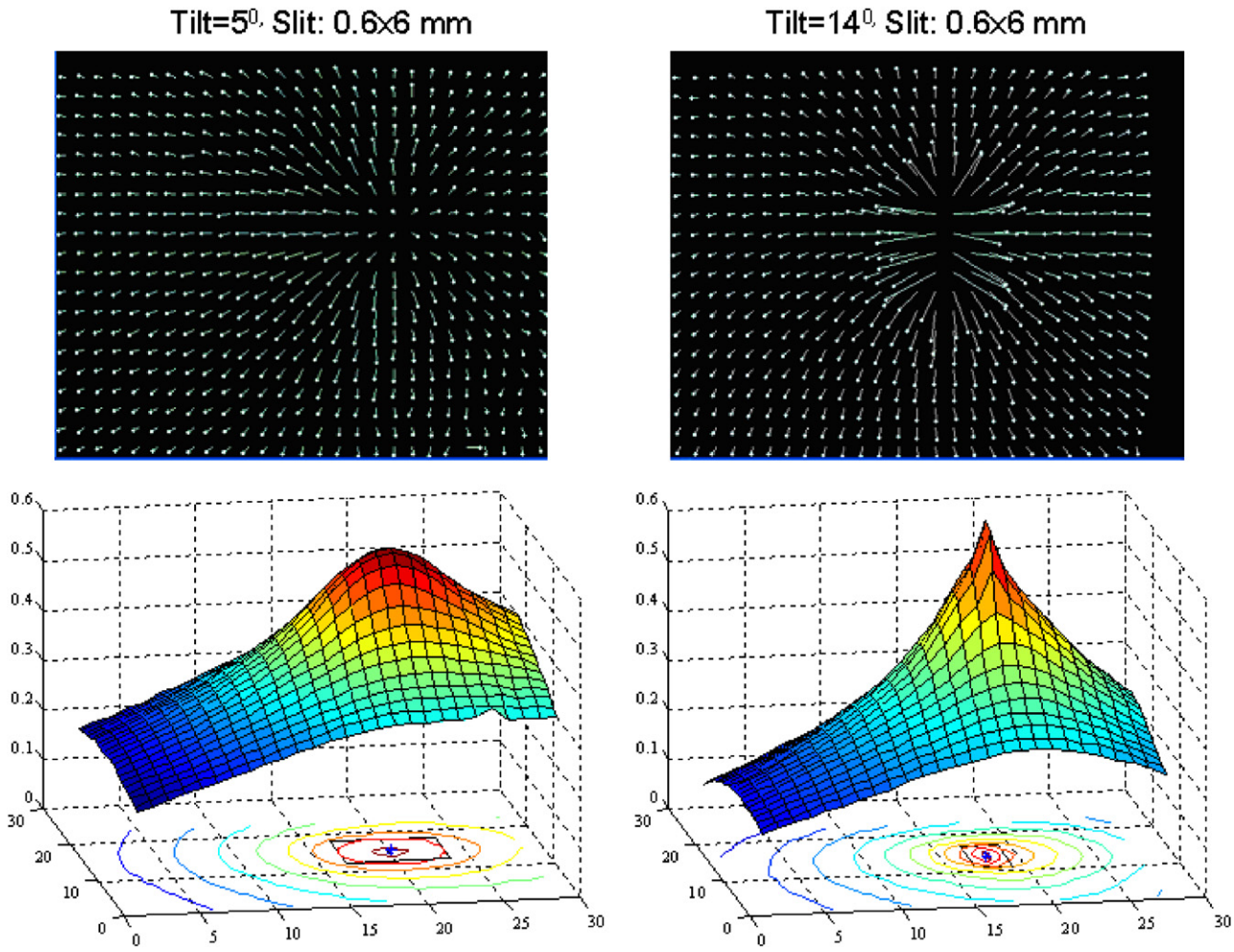

Fig. 5. On the top: slope error maps as measured; below: reconstructed heat-bump surfaces calculated form the measured slope error maps with contour plots of the heat-bump surfaces for two angles of beam incidence (5° and 14°) with the same slit size. The rectangles on the contour plot represent the beam footprint. The surfaces are shifted up to better reveal the contour plots.

4. Surface profile reconstruction

Reconstruction of the surface from gradient fields is a representative of the well-known problem of "shape from shading" [6]. Ideally, the reconstruction of the surface from the gradient field must not depend on the choice of the integration path. The primary difficulty arises from the fact that experimentally obtained gradient fields rarely satisfy the so-called integrability requirement (zero curl or independence of the surface reconstruction from the integration path), and some sort of correction to the gradients is needed in order to rectify the situation.

Let $p(x,y)$ and $q(x,y)$ be the gradient field (the x and y components of slope vector field, respectively) obtained in the experiment. One seeks to reconstruct the surface $h(x,y)$ from these gradients. Let $\{h_x,h_y\}$ denote the x and y components of gradient vector field of the surface $h(x,y)$, which naturally satisfies integrability requirement. Ideally, $\{h_x,h_y\} = \{p,q\}$. In reality, however, due to measurement errors curl(p,q) is not zero, therefore, a correction $\{\varepsilon_x,\varepsilon_y\}$ to the gradients $\{p,q\}$ is sought so that $\{h_x,h_y\} = \{p,q\} + \{\varepsilon_x,\varepsilon_y\}$. The most straightforward approach, and the one that performs well in the presence of a Gaussian noise, is to minimize the least square error function $J(h) = \int\int((h_x-p)^2+(h_y-q)^2)\,dx\,dy = \int\int(\varepsilon_x{}^2+\varepsilon_y{}^2)\,dx\,dy$. The Euler–Lagrange equation leads to the Poisson equation for $h(x,y)$, which results in minimization of the error function $J(h)$ [7]:

$$\nabla^2 \times h = \mathrm{div}(p,q). \tag{1}$$

For p, q, and subsequently h defined on a grid $N_x \times N_y$, Eq. (1) needs to be expressed in the matrix form

$$L \times h = \rho. \tag{2}$$

Here, $\rho = \mathrm{div}(p,q)$ is a column vector of the size N_xN_y formed by using finite differences of the two neighboring grids for each point, h is a column vector representing the surface $h(x,y)$ on the grid also having the size N_xN_y, and L is a square matrix $N_xN_y \times N_xN_y$ that corresponds to the Laplacian operator. L is represented by the kernel [0 1 0; 1 4 1; 0 1 0] (an operator for 2nd-order differentiation for two-dimensional 2-D space) and is modified at the

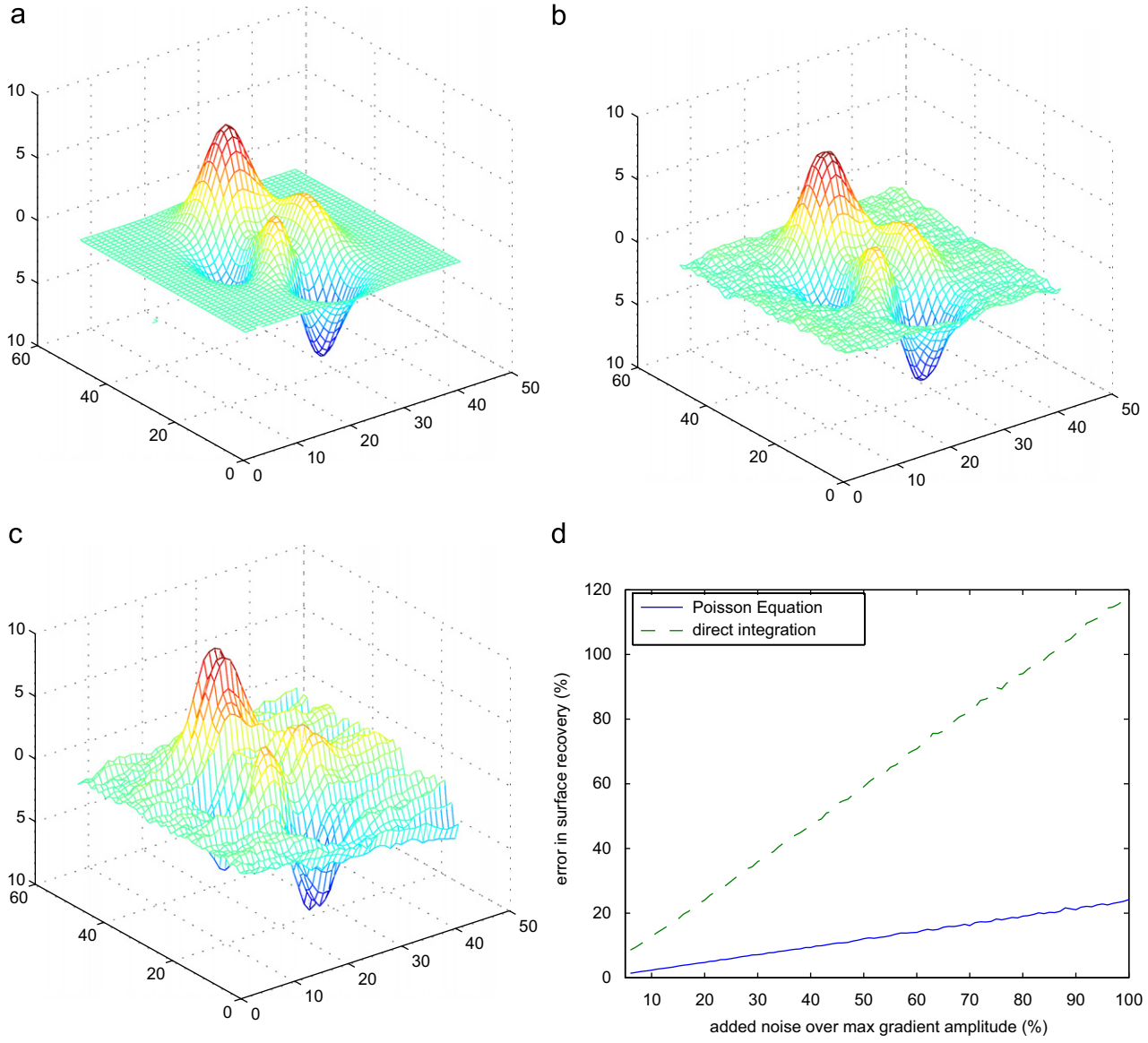

Fig. 6. (a) Initial theoretical surface. (b) Surface reconstruction by solving Poisson equation after 10% of max(|grad h|) noise was added to the gradient field of (a). The RMS error of reconstructed surface is 2.7%. (c) Surface reconstruction via direct integration of x-component of the gradient. RMS error of reconstructed surface is 12.9% of max(|h|). (d) RMS error in reconstructed surface by direct integration (dashed line) and solving the Poisson equation (solid line) versus sigma of the added Gaussian noise of max(|grad h|).

boundaries in accordance with the Neumann boundary condition since the only information available on the surface boundary is the gradient. Finding the reconstructed surface is now reduced to matrix inversion L^{-1} so that the reconstructed surface is obtained by $h = L^{-1}\rho$. Pure Neumann boundary conditions (i.e. only gradient is known at all boundaries) result in singularity of the matrix L. This singularity can be removed by eliminating an arbitrary row and column in L (which is equivalent to fixing a single element of h to zero) followed by usual methods of matrix inversion.

In Fig. 6, we illustrate the performance of this procedure in the presence of Gaussian noise. A scaled parametric Gaussian of two variables (Matlab's peaks function [9]) was used as a model surface shown in Fig. 6(a). We have created the surface's gradient field, grad(h), and added 10% r.m.s. random Gaussian noise to simulate errors occurring in the real experimental environment. Next, we used the Poisson method to reconstruct the surface from the noisy gradient field (Fig. 6(b)). The r.m.s. error of reconstructed surface is only 2.7%. On the other hand, when the surface reconstruction is done via direct integration along x (shown in Fig. 6(c)) of the r.m.s. error of reconstructed surface is 12.9% of max(|h|). The comparison between r.m.s. errors of reconstructed surface by direct integration versus using the Poisson equation as a function of the added Gaussian noise of is shown in Fig. 6(c).

In order to test the surface reconstruction method we reconstructed a flat reflecting surface before and after 80 μrad tilt shown in Fig. 7. The light dot grid array size

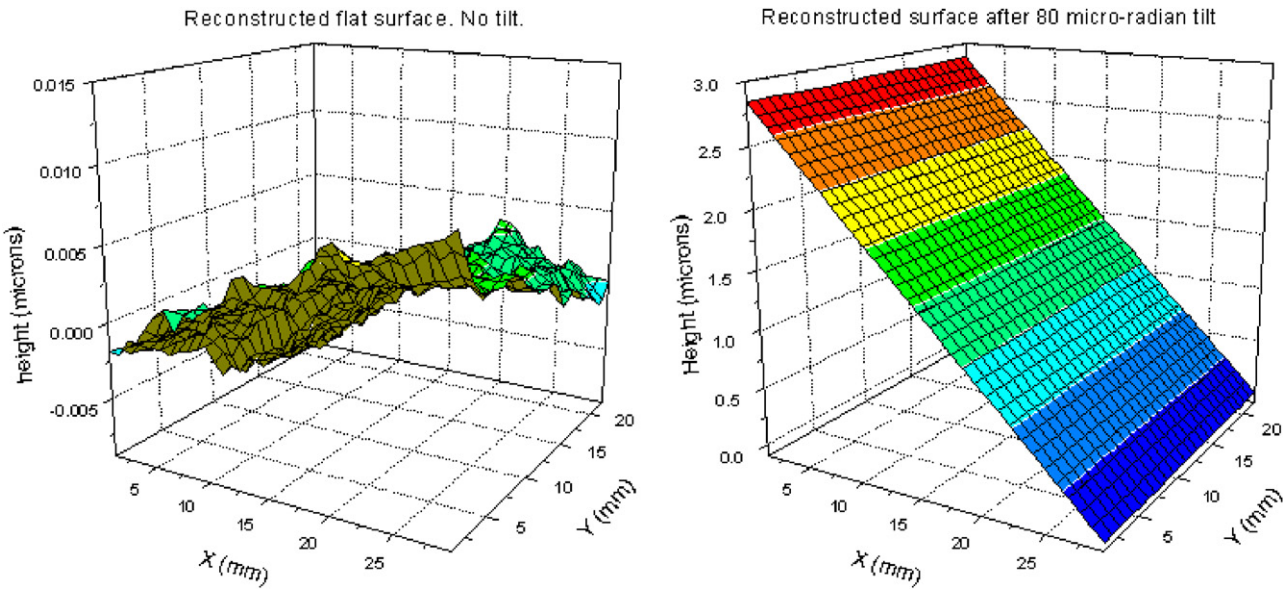

Fig. 7. Reconstructed flat mirror surfaces before and after 80 micro-Radian tilt of the crystal.

was 33×27 dots and the corresponding mirror surface area was $29 \times 22\,\mathrm{mm}^2$. The test showed that the tilted surface is correctly reconstructed.

There are more sophisticated algorithms of surface reconstruction [8] that stabilize the reconstructed surface in the presence of large outliers in the gradient field errors. Surface reconstruction using the Poisson equation (1), however, provides the optimum solution when the error of the measured gradient fields is represented by the simple Gaussian noise.

5. Conclusions

We have demonstrated a new in situ method to measure heat bumps in Si single crystals used in X-ray monochromators. The method is based upon the idea that a distorted reflecting surface will create a distorted image. By measuring the changes in an originally evenly spaced dot array as a result of the distortion of the reflecting surface gives us the gradient vector map of the surface. In order to recover a 3-D surface from the experimentally determined gradient map turned out to be more involved than using a simple integration procedure. As we have shown the measurement errors of the gradient map translate to quite large errors in the reconstructed surface when simple linear integration is used. On the other hand, when more sophisticated mathematical method based on matrix algebra used to reconstruct the surface the propagation of experimental errors will be minimized. Using the Poisson method with the Neumann boundary conditions the shape of the surface of the reflecting crystal can be reconstructed. The technique will be used for the detailed analysis of the heat-bump formation in crystal and multilayer optics with the goal to optimize optics performance in terms of flux and brilliance preservation.

Acknowledgment

This work was based upon research conducted at the Cornell High Energy Synchrotron Source (CHESS), which is supported by the National Science Foundation under award DMR-0225180.

References

[1] D.H. Bilderback, A.K. Freund, G.S. Knapp, D.M. Mills, J. Synchrotron Rad. 7 (2000) 53.
[2] P.Z. Takacs, S.N. Qian, J. Colbert, Proc. SPIE 749 (1987) 59.
[3] P.Z. Takacs, S. Qian, K. Randall, W. Yun, H. Li, Mirror distortion measurements with an in situ LTP, in: A.M. Khounsary (Ed.), Proceedings of the SPIE, vol. 3447, Advances in Mirror Technology for Synchrotron X-Ray and Laser Applications, pp. 117–124.
[4] G. Saeed, M. Lou, Y.M. Zhang, Meas. Sci. Technol. 15 (2004) 389.
[5] P. Revesz, J.A. White, Nucl. Instr. and Meth. A 540 (2005) 470.
[6] B. Horn, Int. J. Comput. Vision 5 (1990) 37.
[7] T. Simchony, et al., IEEE Trans. Pattern Anal. Mach. Intell. 12 (1990) 435.
[8] A. Agrawal, et al., What is the range of surface reconstructions from a gradient field? European Conference on Computer Vision (ECCV), 2006, in press.
[9] Matlab's Peaks function is a parametric Gaussian defined as $f(x,y) = 3(1-x)^2 e^{-x^2-(y+1)^2} - 10\left(\frac{x}{5} - x^3 - y^5\right) e^{-x^2-y^2} - \frac{1}{3} e^{-(x+1)^2-y^2}$.